Two-Phase Electronic Cooling Using Mini-Channel and Micro-Channel Heat Sinks: Part 1—Design Criteria and Heat Diffusion Constraints

Morris B. Bowers
Graduate Student.

Issam Mudawar
Professor and Director.

Electronic Cooling Research Center,
Boiling and Two-Phase Flow Laboratory,
School of Mechanical Engineering,
Purdue University,
West Lafayette, IN 47907

Mini-channel (D = 2.54 mm) and micro-channel (D = 510 μm) heat sinks with a 1-cm^2 heated surface were tested for their high heat flux performance with flow boiling of R-113. Experimental results yielded CHF values in excess of 200 W cm^{-2} for flow rates less than 95 ml min^{-1} (0.025 gpm) over a range of inlet subcooling from 10 to 32°C. Heat diffusion within the heat sink was analyzed to ascertain the optimum heat sink geometry in terms of channel spacing and overall thickness. A heat sink thickness to channel diameter ratio of 1.2 provided a good compromise between minimizing overall thermal resistance and structural integrity. A ratio of channel pitch to diameter of less than two produced negligible surface temperature gradients even with a surface heat flux of 200 W cm^{-2}. To further aid in determining channel diameter for a specific cooling application, a pressure drop model was developed, which is presented in the second part of the study.

Introduction

Technological advances in the electronics industry have resulted in several order of magnitude increases in component concentration at the chip level. Accompanying these advances are significant increases in dissipative heat fluxes; therefore, to accommodate the heat flux demands, new cooling technologies are being developed. Tuckerman and Pease (1981) pioneered high flux electronic cooling with the development of micro-channels. These are small heat sinks of roughly 1-cm square in heated surface area that achieve high single-phase heat transfer coefficients with rectangular channels having very small hydraulic diameter. Unfortunately, tests with water yielded enormous pressure drops at high fluxes (about 1 bar at 181 W cm^{-2}). Additional studies of convective cooling with micro-channels, both numerical (Phillips, 1987; Weisberg et al., 1992) and analytical (Samalam, 1989), have been conducted to determine the channel height and spacing that would achieve optimum thermal performance. Good performances were realized with hydraulic diameters on the order of D = 100 μm; however, successful heat transfer performance was accomplished with pressure drops in excess of 0.69 bar. The higher heat fluxes demanded much greater pressure drops as well as streamwise temperature increases of 15°C or more.

Practical issues associated with an electronic cooling scheme are not only the capability to dissipate a given heat load, but also to reduce both surface temperature and temperature gradients while minimizing pressure drop. For specific applications such as avionic or space systems, it is important to maintain reasonable limits on surface temperature; however, a special emphasis is also placed on reducing the total fluid inventory and pressure drop. This means achieving the cooling goals with both low weight and low pumping power.

With single-phase cooling, there is a linear increase in stream temperature with increasing heat load as illustrated in Fig. 1, where T_s and T_f are the respective surface and fluid temperatures, and this linear temperature rise contributes to greater surface temperature gradients. Phillips (1987) fitted micro-channel heat sinks with compensation heaters in order to reduce these stream-wise temperature gradients. The heaters were located near the channel inlet, where the cooling fluid temperature was low and heat transfer coefficient was high, thus combating the problem of much lower surface temperatures close to the inlet as compared to the exit.

The previous work on micro-channel technology utilized single-phase cooling. Two-phase cooling (i.e., with flow boiling and annular film evaporation) is an alternative mode for micro-channel heat sinking which offers several inherent advantages over single-phase cooling as illustrated in Fig. 1. Uniformity of temperature is better achieved with boiling and evaporation, where the surface temperature, T_s, even for high heat fluxes, is only a few degrees higher than the fluid temperature, T_f, which is equal to the saturation temperature. Also, boiling and

Contributed by the Electrical and Electronic Packaging Division for publication in the JOURNAL OF ELECTRONIC PACKAGING. Manuscript received by the EEPD January 2, 1994; revised manuscript received April 30, 1994. Associate Technical Editor: B. G. Sammakia.

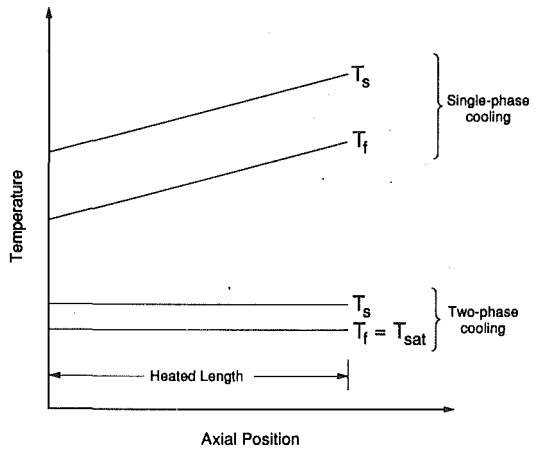

Fig. 1 Comparison of single-phase and two-phase cooling in a uniformly heated tube at the same heat flux and coolant flow rate

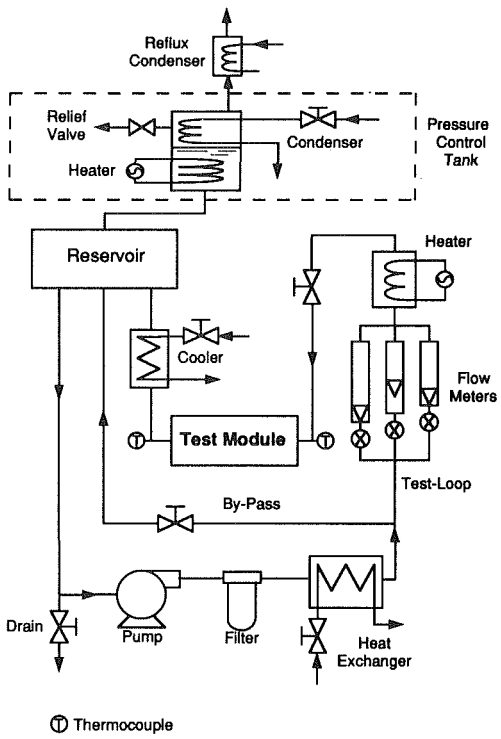

Fig. 2 Flow loop

evaporation facilitate the transfer of heat mainly by latent, as opposed to sensible heat. The latent heat exchange offers the capability of high flux dissipation with very low flow rates; however, vapor production can lead to a significant increase in pressure drop as compared to single-phase flow. An additional constraint associated with any boiling configuration is the critical heat flux, CHF. CHF is the heat flux corresponding to the transition from nucleate boiling to film boiling. This transition causes a drastic drop in the heat transfer coefficient resulting in a large rise in surface temperature that can lead to permanent chip damage.

Making use of the unique advantages offered by two-phase cooling, the present study examined a new high heat flux cooling scheme while placing a special emphasis on issues pertaining to electronic cooling. This scheme consists of flow boiling in both a mini-channel (D = 2.54 mm) and a micro-channel (D = 510 μm) heat sink, where the former is similar in shape to the micro-channel heat sink with the major distinguishing feature of the channel hydraulic diameter being larger by roughly an order of magnitude. Presented in this paper is a brief comparison of experimental results for the pressure drop and CHF characteristics of a mini-channel and a micro-channel heat sink. However, the emphasis of this paper is on establishing criteria and analytical tools for optimizing the geometry of a miniature heat sink. Analytical tools are developed for heat conduction within the heat sink to arrive at the optimum channel spacing and heat sink thickness in dimensionless terms as scaled by the channel diameter. Also, complementing the work reported in this paper is a detailed pressure drop model for a miniature heat sink, which is presented in Part 2 of the present study (Bowers and Mudawar, 1994). It contains the remaining analytical tools that are necessary to determine the optimum channel diameter based upon pressure drop constraints.

Experimental Facility

Tests were conducted with R-113 using the flow loop shown in Fig. 2. The fluid was circulated through the loop using a small (1/10 hp) magnetically-coupled centrifugal pump. The coolant was pumped through a 5 μm filter and then into a heat exchanger where the entire flow was either heated or cooled depending upon the test conditions. Upon exiting the heat exchanger, a portion of the flow, controlled by the by-

Nomenclature

D = channel diameter
G = mass velocity, $G = 4\rho_f Q_T/(N\pi D^2)$
h_{fg} = latent heat of vaporization
k = thermal conductivity
L = heated length of heat sink channel
N = number of channels in heat sink
P = pressure
ΔP = pressure drop
q = heat flux based upon 1-cm^2 heated upper surface of heat sink
q_e = heat flux based upon perimeter encompassed by effective angle
q_m = CHF based upon 1-cm^2 heated upper surface of heat sink
q_p = local heat flux along the channel inside area
$\overline{q_p}$ = mean heat flux based upon channel inside area
$\overline{q_{m,p}}$ = CHF based upon the heated channel inside area
Q_T = total volumetric flow rate of heat sink
R_t' = thermal resistance per unit length
S' = shape factor per unit length
t = thickness of heat sink
t_w = width of cross sectional cell containing one channel
T = temperature
T_s = reference surface temperature used in boiling curves
ΔT_{sub} = liquid subcooling, $T_{sat} - T$
θ = channel circumferential angle
θ_e = effective circumferential angle
ρ = density
σ = surface tension

Subscripts

c = cold
f = liquid
h = hot
i = inlet
m = max (critical heat flux)
p = channel perimeter (inside area)
sat = saturation
sub = subcooled

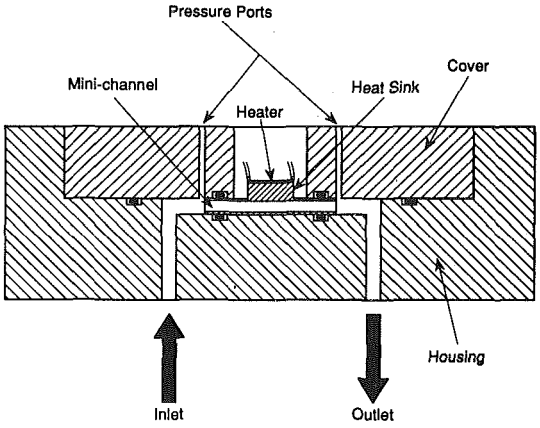

Fig. 3 Cross-section of test module

pass and test loop control valves, entered the test loop while the remaining flow returned to the loop reservoir. Within the test loop, the R-113 entered one of three rotameters for flow rate measurement. The flow meter was followed by a heater for fine adjustment of the fluid temperature. The fluid temperature was measured with a thermocouple that was located in the tubing just upstream of the test module. The R-113 then entered the test module and, upon exiting, the outlet temperature was measured with a thermocouple located in the exit tubing. Leaving the test module, the fluid passed through a cooler which condensed the vapor produced from boiling in the test module. The flow then entered the reservoir where it was mixed with the bypassed fluid.

The fluid in the reservoir was in the liquid phase at all times; however, connected to the top of the reservoir was a pressure control tank, which contained a liquid-vapor mixture. The tank was fitted with both a heater and condenser, thereby allowing control of the entire system pressure through the addition or removal of heat from the two-phase mixture. Also connected to the pressure control tank was a reflux condenser which was used only during deaeration of the fluid.

Test Module. The test module consisted of the heat sink, a G-10 plastic housing, and a G-10 plastic cover as shown in Fig. 3. The housing was machined so that, with the cover in place, either the mini-channel or micro-channel heat sink could be secured in place. The heat sink was press fit as shown in Fig. 3; a combination of the press fit and o-rings located in both the housing and the cover maintained a leak proof seal. The housing contained both inlet and outlet plenums to provide for an even distribution of the flow between the individual heat sink channels as well as even exit mixing. Pressure ports were located in the cover at the inlet and outlet plenums.

Detailed drawings of the mini-channel and micro-channel heat sinks are shown in Figs. 4(*a*) and 4(*b*), respectively. The mini-channel heat sink was fabricated from a single block of oxygen-free copper, with an overall design that consisted of a 10.0 mm square platform protruding from a 28.6 mm square base. Both the platform and the base were 3.18 mm in height; however, the base was made larger to allow room for the o-ring seal. The base contained three channels of 2.54 mm i.d. that ran the entire length of the channel and were equidistantly spaced within a 1-cm width which yielded a channel spacing in terms of the width to diameter ratio of $t_w/D = 1.31$. Silver soldered to the top of the platform was a uniform heat flux thick-film resistor, and located at the center of the platform was a Chromel-Alumel (Type K) thermocouple made from 0.13 mm wire, which provided a reference temperature for the boiling studies. To reduce uncertainties associated with the temperature measurement, the thermocouple was embedded in a 0.81-mm hole that was filled with a thermally-conducting epoxy containing boron nitride.

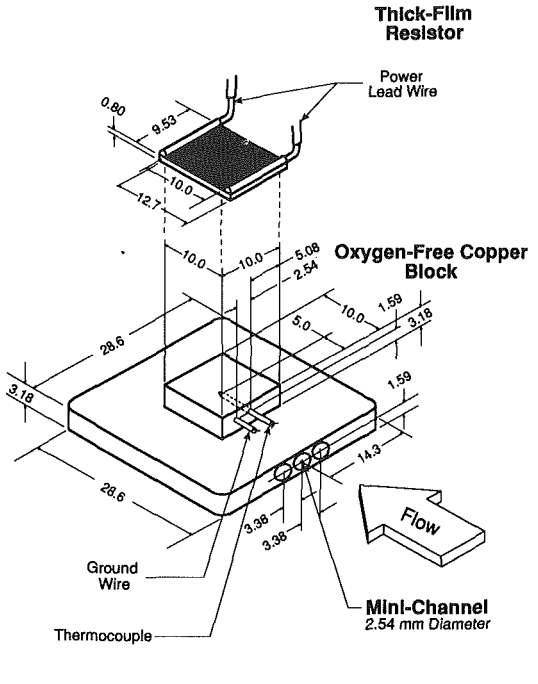

Fig. 4(*a*)

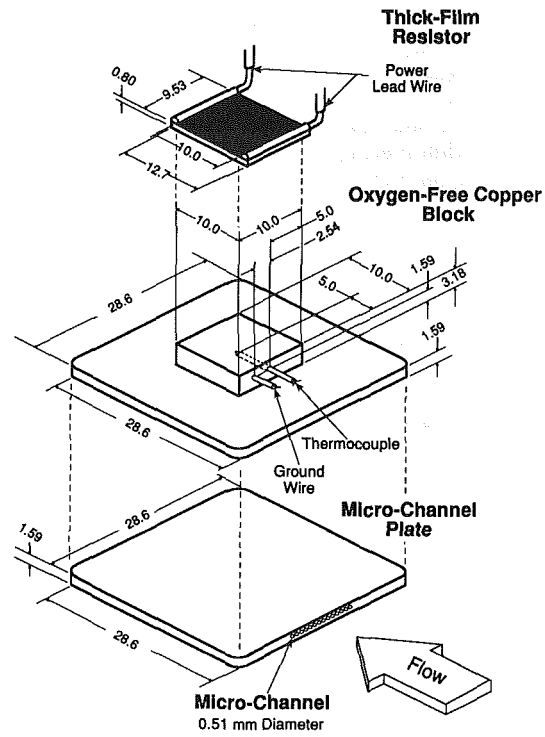

Fig. 4(*b*)

Fig. 4 (*a*) Mini-channel and (*b*) micro-channel heat sink

The platform of the micro-channel heat sink was identical to that of the mini-channel heat sink; however, unlike the mini-channel, the micro-channel heat sink was made from two separate pieces: a top copper block and a bottom nickel plate. The micro-channel plate was fabricated by 3M company with channels of 510 μm i.d. that ran the entire length of the plate and had a channel spacing of $t_w/D = 1.15$. The remaining copper portion of the base served only as a spacer, making

the same test module usable with both heat sinks. The micro-channel plate was attached to the copper block by silver solder. The outer channels of the micro-channel plate were filled with solder at the channel inlets and outlets to assure that the only active channels (a total of 17) were within a 1-cm width below the platform.

Operating Procedure. During a given test, flow rate, heat sink inlet pressure, and the heat sink inlet subcooling were continuously monitored and adjusted, as needed, to maintain the appropriate operating conditions. To obtain boiling data, the power to the heater was manually controlled using a 0-240 Vac variac, with each power setting maintained until steady-state conditions were achieved and the data recorded. The pressure, temperature, and power values were monitored and recorded using a Keithley 500 data acquisition system which was interfaced to a Compaq computer. Steady state was achieved when the standard deviation for 15 values of the heater temperature measured over a 30-s interval was less than 0.2°C; however, this constraint was slightly relaxed at heat fluxes close to CHF due to greater fluctuation in the heater temperature. CHF was easily detected by a sudden unsteady rise in the heat sink temperature.

To ensure that the R-113 was free of dissolved air, the fluid was retained in the closed system at all times, and also, the loop was periodically deaerated. The deaeration procedure was performed by raising the temperature of the circulating fluid above the saturation temperature until the fluid was vigorously boiling. The gaseous mixture was vented to the reflux condenser where the R-113 vapor was condensed and returned into the system while the air and other noncondensable gases escaped to the ambient.

When obtaining boiling data, a heat sink reference temperature was measured with the thermocouple located in each of the heat sinks; however, for the purpose of presenting boiling curves, a temperature that more closely represented the heat sink surface temperature, T_s, was defined. This is the temperature that would correspond to the plane separating the base of the heat sink from the top platform. T_s was calculated by assuming one-dimensional heat conduction between the plane of the thermocouple and the reference plane for T_s.

Experimental Uncertainty. Uncertainty associated with measurement of differential pressure across the heat sink was estimated to be less than 5 percent for pressures smaller than 0.02 bar and less than 1 percent for the higher values of differential pressure. Uncertainty in the measurement of absolute pressure at the inlet to the heat sink was 1 percent. Thermocouples were estimated to have uncertainties smaller than 0.2°C, with the exception of the heat sink thermcouple. Additional error was associated with this particular thermocouple due to the large temperature gradients encountered at high heat fluxes; this error was estimated to be 1.2°C for a heat flux of 200 W cm^{-2}. Flow rate measurement yielded uncertainty of less than 4 percent with the greatest being for flow rates less than 34 ml min^{-1} (0.009 gpm).

The supplied heat flux was determined from the electrical power supplied to the thick film resistor, which was measured with an uncertainty of less than 1 percent. Heat losses were estimated to be less than 3 percent; therefore, no adjustment for losses were made in calculating the heat flux. The heat loss was determined numerically assuming free convection boundary conditions for the exposed surfaces of the test module and zero contact resistances between the G-10 plastic and heat sink, thereby yielding a very conservative estimate of heat loss. Numerical predictions were also performed for axial conduction within the heat sink for locations in the flow stream directionly upstream and downstream of the 1-cm heated width. For the mini-channel, upstream axial conduction was at most 2.5 percent as compared to 10 percent for the downstream conduction,

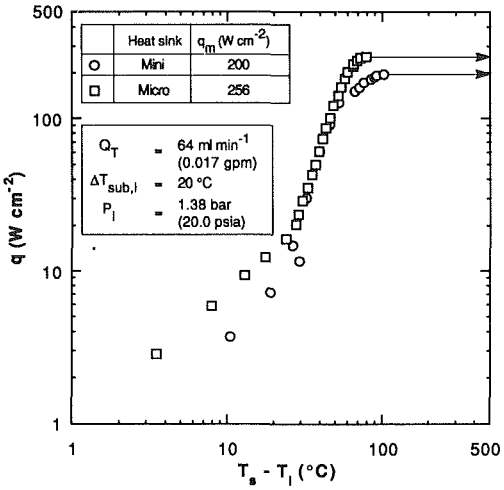

Fig. 5 Comparison of mini- and micro-channel boiling curves for a flow rate of 64 ml min^{-1} and 20°C inlet subcooling

and estimates for the micro-channel were at most 4.5 and 12 percent for upstream and downstream conduction, respectively.

Experimental Results

Experiments were performed to determine both the hydrodynamic and heat transfer characteristics of the fluid in the mini- and micro-channel heat sinks. Special emphasis was placed on obtaining boiling curves for heat fluxes up to CHF while, simultaneously, obtaining two-phase pressure drop data. Tests were conducted at an inlet pressure of 20 bar over a range of inlet subcooling from 10 to 32°C and flow rates from 19 to 95 ml min^{-1} (0.005 to 0.025 gpm). A comparison of boiling curves for the mini- and micro-channel heat sinks at a flow rate of 64 ml min^{-1} is shown in Fig. 5. The curves are characterized by a distinct offset in the single-phase region with the micro-channel exhibiting a superior heat transfer performance; however, within the nucleate boiling regime, the distinction is less discernable. The similar behavior in the nucleate boiling regime would be expected since the total heat transfer areas are approximately equal with an area ratio of the micro-channel relative to the mini-channel of 1.14. Approaching CHF, the heat transfer coefficient dropped off more with the mini-channel than with the micro-channel, before reaching a maximum heat flux of 200 W cm^{-2} as compared to 256 W cm^{-2} for the micro-channel. The micro-channel yielded this 28 percent increase in CHF over the mini-channel at the expense of a much larger pressure drop as shown in Fig. 6. Within the single-phase region, pressure drop for both heat sinks was low ($\Delta P < 0.02$ bar); however, there was a large difference in pressure drop in the boiling region. This was especially true for higher fluxes above 100 W cm^{-2}, where the pressure drop for the micro-channel climbed to values in excess of 0.30 bar while the mini-channel pressure drop remained below 0.03 bar. The comparable heat transfer behavior contrasted with the drastic differences in pressure drop definitely warrant the need for analytical tools to predict both CHF and pressure drop for mini- and micro-channel heat sinks.

Additional experimental results and a more detailed discussion of the heat transfer characteristics of the heat sinks can be found in another study by Bowers and Mudawar (1994). This study yielded the following CHF correlation for mean heat flux along the channel wall:

$$\frac{\overline{q_{m,p}}}{Gh_{fg}} = 0.16 \left(\frac{\sigma\rho_f}{G^2 L}\right)^{0.19} \left(\frac{L}{D}\right)^{-0.54}, \quad (1)$$

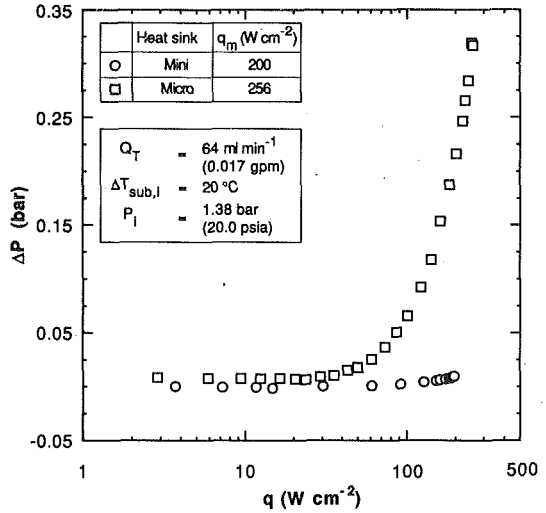

Fig. 6 Comparison of mini-channel and micro-channel pressure drops

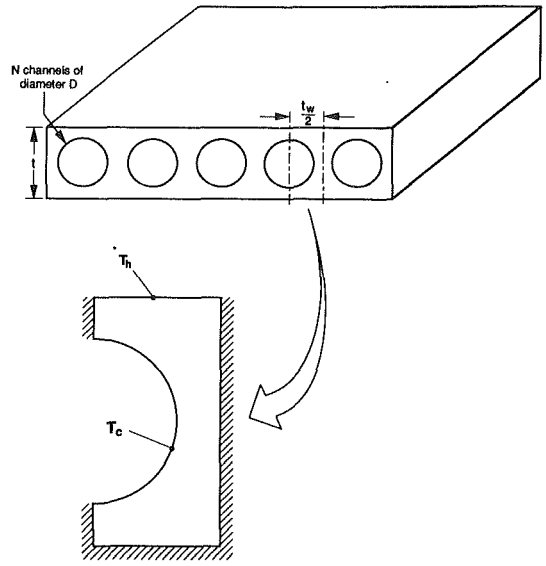

Fig. 7 Schematic of heat sink and definition of half-cell geometry and boundary conditions

which is applicable for both mini- and micro-channel heat sinks. This correlation, which has a mean absolute error of 3.0 percent, fulfills only one aspect of cooling scheme design; however, to complement the correlation, analytical tools are also needed to optimize heat sink design for a specific application such as electronic cooling.

Heat Sink Geometry

For a specific cooling application employing a mini-channel or micro-channel heat sink, the question arises to as what the optimum channel diameter should be, and even more specifically, how the channels should be spaced within the heat sink to provide the best transfer of heat to the cooling fluid. It is first necessary to define specific criteria for an optimum design; this should then be followed by the development of analytical tools for addressing each criterion.

For optimization of a heat sink's geometrical parameters such as thickness, channel diameter, and channel spacing, it is paramount to satisfy the following criteria:

(1) minimize the thermal resistance between the upper surface and coolant channel wall, thus reducing the device temperature;
(2) maintain a relatively isothermal upper surface to avoid temperature gradients that may be damaging to electronic components;
(3) minimize the heat flux present at the cooling channel wall for a given heat flux at the upper surface, thereby maximizing the total heat load for which CHF occurs;
(4) minimize pressure drop; and
(5) minimize total coolant flow rate.

In the following sections, analytical tools will be developed and employed to specifically address criteria (1) through (3); the last two criteria will be discussed in Part 2 of this paper (Bowers and Mudawar, 1994).

Thermal Resistance Across Heat Sink. When analyzing heat conduction in a two-dimensional system, it is convenient to define the thermal resistance per unit length, R_t', as

$$R_t' = \frac{1}{kS'} \tag{2}$$

where S' is the shape factor per unit length. The half-cell has hot and cold isothermal boundaries T_h and T_c, respectively, and the shape factor per unit length in the direction of fluid flow, S', is defined as

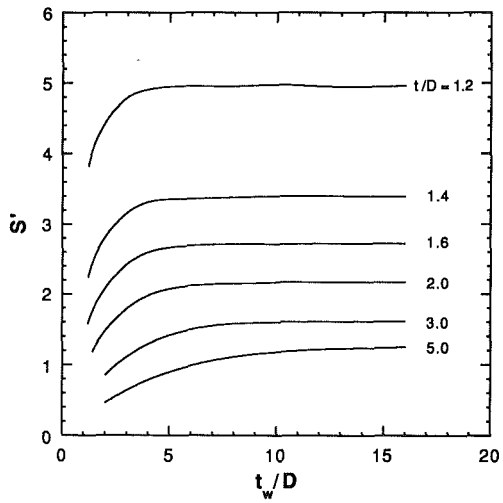

Fig. 8 Shape factors for different heat sink thicknesses and cell widths

$$S' = \frac{q\left(\frac{t_w}{2}\right)}{k(T_h - T_c)}. \tag{3}$$

Referring to Fig. 7, a mini- or micro-channel heat sink can be defined as having N circular channels each being contained within a rectangular cell of cross-sectional dimensions t_w and t. The simplest geometry for thermal resistance analysis, based upon thermal and geometrical symmetry, is a one-half cell ($t_w/2 \times t$). To evaluate the thermal resistance for heat sinks of varying cell widths and thicknesses, a parametric study was performed for dimensionless thicknesses, t/D, ranging from 1.2 to 5.0 and cell widths, t_w/D, from 1.1 to 16.

Figure 8 shows the numerical shape factor results determined from Eq. (3) using a finite element code. A reduction in heat sink height thickness, t/D, yields an increase in shape factor, which would correspond to a decrease in thermal resistance between the channel wall and the heat sink top surface. The opposite is true for increasing channel spacing t_w/D. As the cell width increases, the shape factor also increases; however, it reaches a maximum value and further increases in width yield no change in shape factor. These trends are made clearer

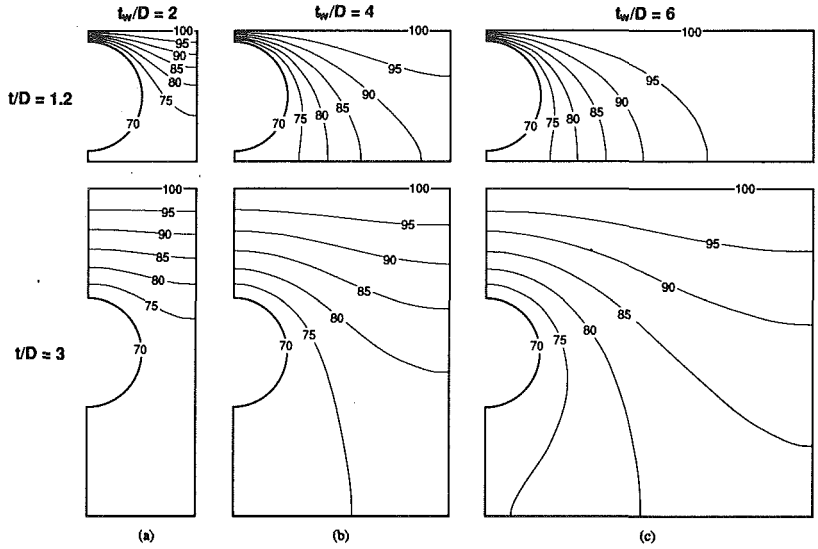

Fig. 9 Isotherm plots for two heat sink thicknesses and dimensionless cell widths of (*a*) 2, (*b*) 4, and (*c*) 6

by the isotherm plots given in Fig. 9 for $T_h = 100°C$ and $T_c = 70°C$. At $t/D = 1.2$, the shape factor increases from 4.2 to 4.9 for an increase in cell width from $t_w/D = 2$ to 4. The increase in shape factor corresponds to the isotherms being pulled further around the channel wall, thus making greater use of the area around the channel for heat flow. A further increase in cell width to $t_w/D = 6$ results in only a slight change in the isotherms around the channel. The effect of increasing heat transfer area at the upper surface is negated by the increasing length of conduction path, which is why the shape factor becomes insensitive to further increases in cell width. The major distinguishing characteristic for an increase in thickness from $t/D = 1.2$ to 3 is the increased length of conduction path from the upper surface to the channel wall. The longer conduction path increases the thermal resistance and, as expected, reduces the shape factor.

Figure 8 shows that the near-asymptotic value of S' is attained at larger cell widths with increasing values of thickness. For the cell width of $t_w/D = 6$, isotherms are pulled further around the channel wall than with $t/D = 1.2$, thus making greater use of the channel wall area for heat transfer.

For a more complete examination of the shape factor, a comparison was made with an analytical solution for a geometry similar to that of the present study with the exception of the lower surface being a semi-infinite body (see Fig. 10). Besides its usefulness as a reference case for the present study, this geometry has practical merit. It facilitates reducing thermal resistance, by decreasing the thickness of metal above the channels, while relying on much thicker metal below the channels for structural integrity. The analytical prediction (Kutateladze, 1963) of shape factor between the upper surface and the channel wall for a half-cell of width $t_w/2$ in the semi-infinite geometry is

$$S' = \frac{\pi}{\ln\left[\left(\frac{2t_w}{\pi D}\right)\sinh\left(\frac{\pi t}{t_w}\right)\right]}. \quad (4)$$

A comparison of shape factors for the finite heat sink geometry of the present study with those for the semi-infinite geometry is given in Fig. 10. For $t/D = 5$ or greater, the semi-infinite model closely predicts the shape factor for the finite heat sink due to the diminishing role of the area below the channel for large cell thicknesses. It can further be concluded that for a

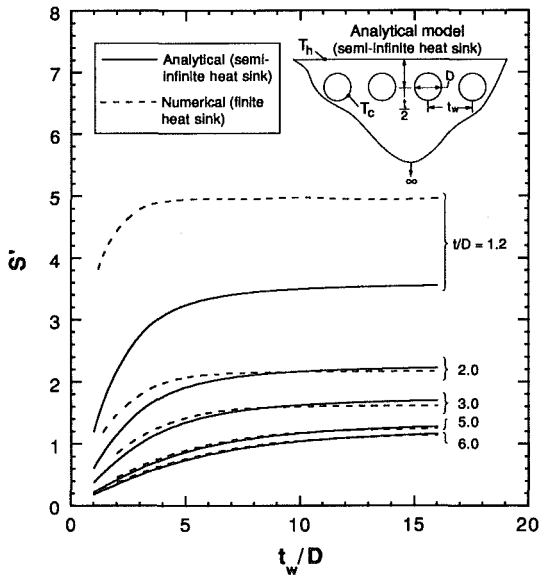

Fig. 10 Comparison of numerically determined shape factors for finite heat sink geometry of present study with analytically determined values for semi-infinite heat sink

height of $t/D = 5$, increasing the depth below the channel would have no effect on the shape factor or heat transfer.

Based upon the shape factor study alone, it could be concluded that to achieve a minimum thermal resistance between the surface and channel wall, the heat sink's thickness, t/D, should be minimized, although a value of about 1.2 should be imposed for structural considerations; no detailed structural calculations were attempted in the present study. Also, the conductive resistance is minimized for t_w/D values of 4.9 or greater. However, reducing the conductive resistance alone only addresses one of the optimization criteria. It does not address the issue of reducing channel wall heat flux nor the effect of nonisothermal boundaries on channel spacing.

Isothermal Versus Constant Heat Flux Boundary. The shape factor analysis in the previous section examined isothermal boundaries at both the top surface and along the channel wall. The isothermal boundary assumption for the

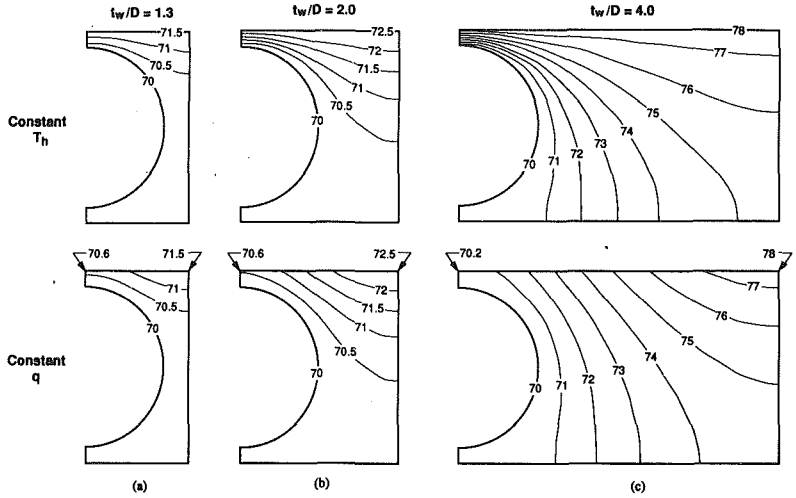

Note: All temperatures are in °C and the constant heat flux at the upper surface in the three lower cases is 200 W cm^{-2}. The three lower cases are for a copper heat sink with k = 386 W m^{-1}K^{-1}.

Fig. 11 Isotherms for constant temperature and for constant heat flux at top surface for t/D = 1.2 and t_w/D = (*a*) 1.31 (mini-channel geometry of present study), (*b*) 2, and (*c*) 4

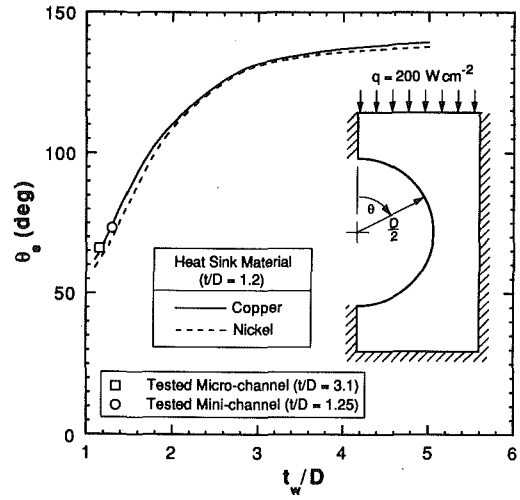

Fig. 12 Circumferential angle through which 95 percent of the supplied heat enters the copper and nickel heat sink with t/D = 1.2

channel wall is justified for channels undergoing boiling; however, heat sinks for most practical applications, and specifically for the cases studied, are more closely approximated by a constant heat flux at the top surface. Figure 11 compares isotherm plots for t/D = 1.2 for a constant heat flux boundary, q = 200 W cm^{-2}, at the upper surface with plots for constant temperature boundaries between the same minimum and maximum temperatures. It should be further noted that the case (*a*) represents the geometry of the mini-channel heat sink studied experimentally. Comparing the isothermal and constant heat flux cases shows that the smallest cell widths (mini-channel geometry) most closely resemble each other with a maximum temperature difference along the upper surface of less than 1°C for the constant heat flux case compared to 7.8°C for t_w/D = 4. Thus, reducing temperature gradients along the upper surface requires minimizing the cell width. This conclusion contradicts the results for reducing the conductive resistance; however, analysis of the wall heat flux is necessary to completely determine the optimum channel spacing based upon the established criteria.

Effective Heat Flux. To complete the analysis for determining channel spacing, the heat flux distribution along the channel wall was investigated. To accomplish this goal, an effective angle, θ_e, was defined as the circumferential angle that encompasses 95 percent of the total heat flow into the channel wall as shown in Fig. 12. This angle was determined from the following equation:

$$0.95\, q\, \frac{t_w}{2} = \int_0^{\theta_e} q_p(\theta)\, \frac{D}{2}\, d\theta, \tag{5}$$

where $q_p(\theta)$ is the heat flux through a differential element $D/2\ d\theta$. Using a finite element code, the effective angle was determined for a range of cell widths from t_w/D = 1.1 to 5 and a t/D = 1.2 which is the thickness corresponding to minimum conductive resistance while satisfying the structural integrity criterion, $t/D \geq 1.2$. The top surface heat flux was assumed constant at 200 W cm^{-2}, and the channel wall was assumed isothermal at 70°C. Also, since mini- and micro-channel plates are typically made from copper or nickel, including those tested in the present study, effective angles for both materials were calculated.

Figure 12 shows a drastic rise in effective angle, from 60 to 100 degrees, corresponding to an increase in cell width from t_w/D = 1.1 to 1.7. However, with further increases in width, the effect of greater channel spacing diminishes, yielding an angle of about 140 degrees at t_w/D = 5. The effective angles for nickel and copper compare very closely over the entire range of cell widths examined. The effective angle for the mini-channel with t/D = 1.2 was determined to be 74 degrees as compared to 66 degrees for the micro-channel. The tested micro-channel heat sink was of greater thickness, t/D = 3.1; however, the calculated value for this ratio, falling directly on the nickel curve corresponding to t/D = 1.2, illustrates a lack of sensitivity to heat sink thickness as well as heat sink material when determining the effective angle. To fully utilize these results in determining the optimum channel spacing for a heat sink, it is paramount to determine the magnitude of the heat flux along the channel wall for a given heat flux at the upper surface. Minimizing the channel heat flux is a crucial measure in the prevention of CHF inside the channel.

Writing an energy balance for the half-cell yields

$$0.95\, q t_w = q_e\, \theta_e D, \tag{6}$$

where q_e is the mean heat flux concentrated along the perimeter encompassed by the effective angle. Rearranging Eq. (6),

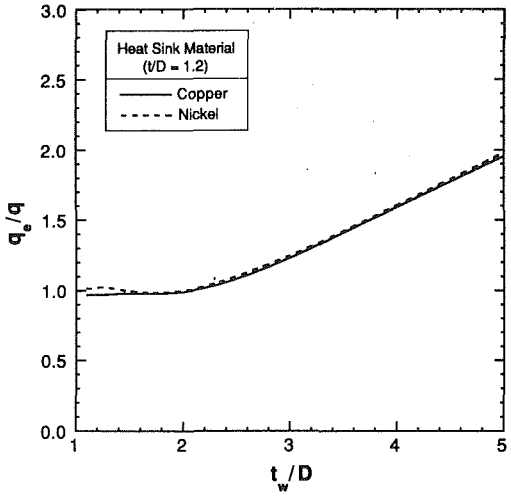

Fig. 13 Ratio of mean heat flux along the perimeter of the channel encompassed by the effective angle to upper surface heat flux for copper and nickel heat sinks

$$\frac{q_e}{q} = 0.95 \frac{t_w/D}{\theta_e}. \tag{7}$$

To optimize the design of a mini- or micro-channel heat sink based upon reducing the heat flux along the channel wall, the ratio q_e/q must be minimized. According to equation (7), this goal can be accomplished by reducing the ratio of dimensionless cell width to effective angle. Figure 13 shows q_e/q assumes a constant minimum value of about 1.0 for all values of t_w/D less than two, above which q_e/q increases drastically with increasing cell width. Thus, if the channel spacing is too large, the heat flux concentrated along the channel wall will be much greater than the heat flux applied at the upper surface.

It is apparent from the current analysis that for an optimum channel spacing, the ratio of cell dimensionless width to channel diameter, t_w/D, should be maintained less than about two. This constraint satisfies the criteria for both maintaining a low heat flux along the channel wall as well as reducing the temperature gradient along the upper surface of the heat sink. To decrease the thermal resistance between the upper surface and channel wall while maintaining reasonable structural integrity, the required thickness is $t/D \approx 1.2$. Adherence to these constraints will yield a heat sink design that achieves optimum performance with respect to transferring the heat supplied at the upper surface to the cooling fluid. However, to complete the heat sink design, the channel diameter must be determined based upon flow rate and pressure drop criteria. The remaining analytical tools to complete the design of the heat sink for electronic cooling is found in Part 2 of this study (Bowers and Mudawar, 1994).

Conclusions

A study was conducted to develop analytical tools for optimizing the design of mini-channel and micro-channel heat sinks for electronic cooling. Emphasis was placed on analyzing thermal conduction within the heat sink to determine the optimum channel geometry based upon dimensionless cell width and heat sink thickness. Key findings from the study are as follows:

(1) Mini- and micro-channel heat sinks are capable of achieving heat fluxes in excess of 200 W cm^{-2} with both low flow rates and low pressure drops as required for electronic cooling.
(2) A dimensionless heat sink thickness, t/D, of about 1.2 is a good compromise between maintaining a low thermal resistance and providing adequate structural strength.
(3) Dimensionless channel spacing, t_w/D, in heat sinks designed to dissipate fluxes of about 200 W cm^{-2} should be smaller than 2 in order to minimize surface temperature gradients and to guard against premature CHF in the channel due to high channel heat flux for a given heat flux supplied at the upper surface of the heat sink.

Acknowledgment

The authors thank Mr. Kenneth Thompson of 3M Industrial and Electronics Sector Laboratories for providing the micro-channel heat sink for the present study.

References

Bowers, M. B., and Mudawar, I., 1994, "Two-Phase Electronic Cooling Using Mini-Channel and Micro-Channel Heat Sinks: Part 2—Flow Rate and Pressure Drop Constraints," ASME JOURNAL OF ELECTRONIC PACKAGING, Vol. 116, pp. 298-305.

Bowers, M. B., and Mudawar, I., 1994, "High Flux Boiling in Low Flow Rate, Low Pressure Drop Mini-channel and Micro-channel Heat Sinks," *International Journal of Heat and Mass Transfer*, Vol. 37, pp. 321-332.

Kutateladze, S. S., 1963, *Fundamentals of Heat Transfer*, Arnold Ltd., London, England, p. 92.

Phillips, R. J., 1987, "Forced-Convection, Liquid-Cooled Microchannel Heat Sinks," M.S. thesis, Department of Mechanical Engineering, Massachusetts Institute of Technology, Cambridge, MA.

Samalam, V. K., 1989, "Convective Heat Transfer in Microchannels," *Journal of Electronic Materials*, Vol. 18, pp. 611-617.

Tuckerman, D. B., and Pease, R. F. W., 1981, "High-Performance Heat Sinking for VSLI," *IEEE Electron Device Letters*, Vol. EDL-2, pp. 126-129.

Weisberg, A., Bau, H. H., and Zemel, J. N., 1992, "Analysis of Microchannels for Integrated Cooling," *International Journal of Heat and Mass Transfer*, Vol. 35, pp. 2465-2474.